Supplement of Atmos. Meas. Tech., 15, 4171–4194, 2022
https://doi.org/10.5194/amt-15-4171-2022-supplement

Atmospheric Measurement Techniques
Open Access
EGU

Supplement of

Retrieval of the sea spray aerosol mode from submicron particle size distributions and supermicron scattering during LASIC

Jeramy L. Dedrick et al.

Correspondence to: Lynn M. Russell (lmrussell@ucsd.edu)

Contents of this file

1. Text S1 to S3
2. Figures S1 to S5
3. Table S1 to S6

Text S1. Differentiating Sea Spray Aerosol from Saharan Dust

Absorbing particle influences from dust and other non-marine/continental aerosol were screened from the dataset using the sub-10 μm single-scattering albedo (SSA). The SSA is defined as

$$SSA\ (\lambda) = \frac{b_{sca}(\lambda)}{b_{sca}(\lambda)+b_{abs}(\lambda)}, \quad \text{(S1)},$$

where b_{sca} and b_{abs} are the scattering and absorption coefficients, respectively. Sea salt aerosol typically have a high SSA (~1), while the greater absorbance properties of dust and biomass burning decrease SSA to lower values (0.8 – 0.9) (Muller et al., 2011; Wu et al., 2020; Zuidema et al., 2018). Observational estimates of Saharan dust SSA provide a range of 0.91 – 0.97 for wavelengths between 400 and 550 nm (Di Biagio et al., 2019; Von Hoyningen-Huene et al., 2009; Haywood et al., 2003) and a mean across these wavelengths of 0.95. Due to the predominantly coarse sizes of sea salt and dust, both are expected to have low scattering angstrom exponent values (SAE < 1) (Delene and Ogren, 2002). We therefore distinguish between these two types of aerosol by identifying the regime in which both the SSA is high (~ 1) and the SAE is low (< 1) for sea salt dominated periods.

To estimate SSA, NEPH scattering was adjusted to match the PSAP wavelength of 470 nm using the sub-10 μm SAE at 450-550 nm as described by De Faria et al. (2021). We note that the absorption and scattering coefficients were measured at different relative humidity during LASIC (PSAP RH < 25%, Zuidema et al. 2018; NEPH RH = 55%). These differences may lead to overrepresentation of the SSA due to the larger NEPH humidity, but it provides a baselevel estimate of the parameter that can be used to distinguish the aerosol types. The SSA estimate was calculated for the full 2-h LASIC dataset (April 2016 – October 2017), which captures both the background (November – May) and biomass burning (June – October) seasons. The results relating the SSA and SAE are provided in Fig. S3. For non-marine periods (periods that did not meet criteria described in Sect. 2.2), the SAE tends toward larger values (> 1) and lower SSA (< 0.9). The average SAE and SSA during LASIC marine periods were 0.66 ± 0.15 and 0.97 ± 0.02, respectively, while non-marine SAE and SSA were 0.96 ± 0.3 and 0.89 ± 0.03.

Based on these observations, we chose to further screen periods for the LASIC sea spray retrieval using an SSA threshold of 0.95. This threshold value is within the variability of the average SSA for LASIC marine periods and is consistent with the value observed for marine times at an island site periodically influenced by regional pollution (De Faria et al., 2021) and the observed average of Saharan dust SSA (Di Biagio et al., 2019; Von Hoyningen-Huene et al., 2009; Haywood et al., 2003).

Text S2. Retrieval Sensitivity to Refractive Index

The sensitivity of the sea spray mode retrieval to different sea salt refractive indices (*m*) was evaluated by selecting values that represent the range of nephelometer inlet relative humidity. *m* values were selected in the range of 1.4 + 0i to 1.6 + 0i. This range was based on laboratory and modelling experiments of *m* and Mie scattering of sea salt aerosol at varying relative humidity between < 40% (dry) to > 75% (wet) (Randles et al., 2004; Bi et al., 2018; Wang and Rood, 2008; Saliba et al., 2019) (Table S1). For the purposes of these tests, we assumed the sea salt particles are largely inorganic mixtures with organic components contributing minor if not offsetting *m* differences. The imaginary component of *m* was neglected under the assumption that the clean marine criteria and single-scattering albedo restrictions limited influences of absorbing contributions from non-marine organics and mineral dust and this value is often quite small ($< 10^{-6}$; Wang and Rood, 2008; Randles et al., 2004; Bi et al., 2018). We also assumed that the wavelength dependence of *m* in the visible light range relevant to the nephelometer scattering (450 – 700 nm) is weak (Bi et al., 2018).

Small differences between retrievals using different *m* were observed for the sea spray size distribution fit parameters, and mass correlations (Table S2). The retrieved sea spray mass concentrations using *m* that represent humidified and wet conditions (1.4 + 0i, 1.45 + 0i) were lower on average than those using a "dry" *m* (1.55 + 0i, 1.6 + 0i), but they were within the range of variability for dry *m*. Retrieved sea spray mass correlations with submicron chloride and supermicron scattering were slightly higher when simulating Mie scattering with *m* assumed under more humid conditions (1.45 + 0i, 1.5 + 0i), potentially reflecting a more accurate sea spray retrieval when the simulated scattering is comparable in RH to the measured scattering (average RH = 55 ± 10 %) and UHSAS size distribution measurements (RH = 55 ± 8%). The sea spray mass correlations with wind speed for all *m* did not exceed 0.2, but the most wet *m* (1.4 + 0i) and driest *m* (1.6 + 0i) cases had a lower correlations. The chloride and scattering sea spray tracer correlations are higher when using *m* of 1.45 + 0i and 1.5 + 0i. Even though the changes between the retrieved fit parameters and tracer correlations do not vary substantially, we selected an *m* value of 1.45 + 0i to simulate the sea spray scattering in our Mie calculations, which is assumed to appropriately reflect the sea spray refractive index for salt particles at 55% RH.

Text S3. Estimate of Humidified Sea Spray Particle Density

Size distribution and scattering measurements were not collected under standard dry conditions (RH < 40%) during LASIC, meaning dry particle density assumptions could not be applied in the retrieval of sea spray size distributions using scattering. We instead estimate the sea spray particle density using reported density values for sea spray aerosol and water (Table S3), and a mass-based density mixing rule (Wang and Rood, 2008; Tang et al., 1997), which is represented as,

$$\frac{1}{\rho} = \sum_i \frac{\varepsilon_{m,i}}{\rho_i} \quad \text{(S2).}$$

ρ is the solution density, ρ_i is the density of material *i*, and $\varepsilon_{m,i}$ is the mass fraction of material *i*. Because the measured particles were sampled from high ambient relative humidity (88 ± 8%) before being measured by the nephelometer (55 ± 10%), efflorescence (dehydration) effects needed to be considered.

We used efflorescence hygroscopicity sea spray mass fractions reported for NaCl and complex salt mixtures that included organic and inorganic species at relative humidity intervals within the mean and uncertainty of the nephelometer (45%, 55%, and 65%; Table S4) and determined solution densities (Table S5). The three densities at 45%, 55%, and 65% relative humidity were then used to retrieve sea spray size modal properties (Table S6). Overall, there were no significant differences in the mass, diameter, and widths for each of the densities tested. We therefore take the solution density assumed to be estimated at the average nephelometer and size distribution relative humidity (RH = 55%, ρ = 1.3 g cm^{-3}) as the density value used to retrieve the sea spray mass size distribution.

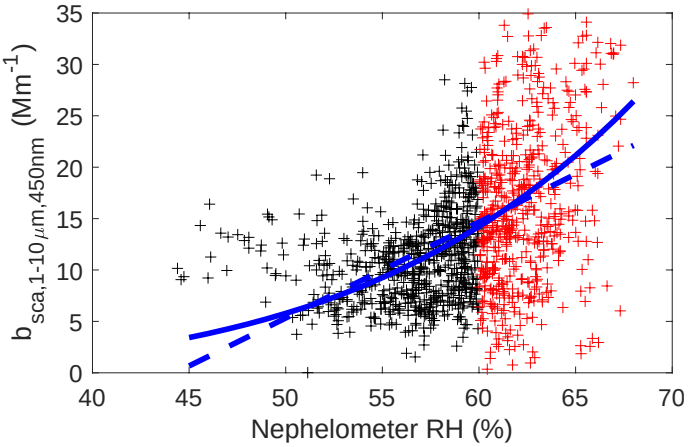

Figure S1. Scatter plot of nephelometer inlet humidity and supermicron scattering at 450 nm (Mm^{-1}). The delineation of black and red symbols indicates the restriction used for applicable UHSAS-NEPH sea spray mode retrieval (Section 2.1.2). Linear (dashed blue line) and power law (solid blue line) fits have been applied to the data.

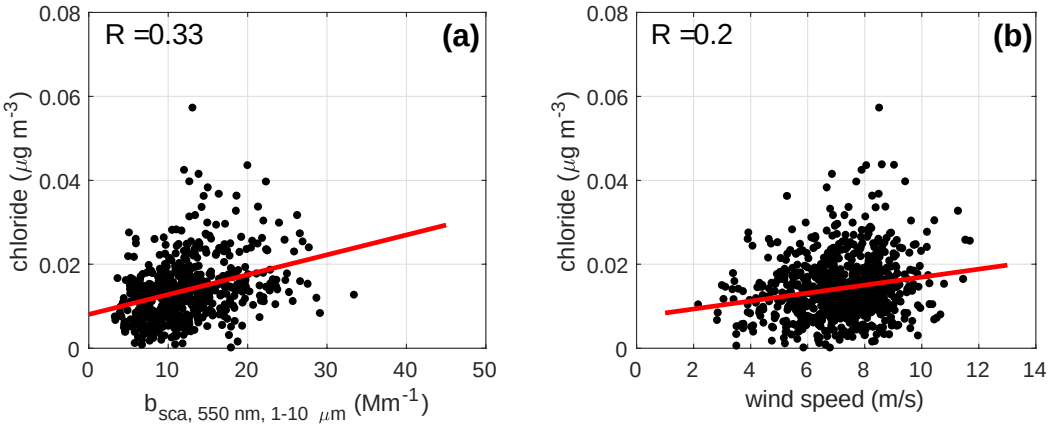

Figure S2. (a) Nephelometer supermicron scattering at 550 nm, and (b) wind speed correlations with ACSM chloride concentrations for the period of January 2017 – May 2017 during LASIC. Linear regressions are fit to the data (solid lines) and Pearson correlation coefficients are provided at top left of each panel ($p < 0.05$).

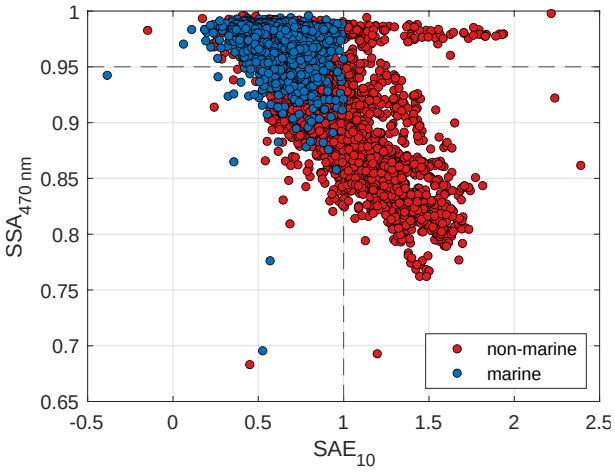

Figure S3. Scatter plot of the 450-700 nm sub-10 µm scattering Angstrom exponent (SAE_{10}) and the 470 nm single-scattering albedo ($SSA_{470\ nm}$). Blue circles represent measurements that meet the clean marine criteria identified in Section 2.2, while orange circles are non-marine times. The dashed vertical line marks an SAE_{10} value of 1 (criteria for clean marine screening) and the dashed horizontal line marks $SSA_{470\ nm}$ 0.95 (criteria to distinguish sea salt from dust).

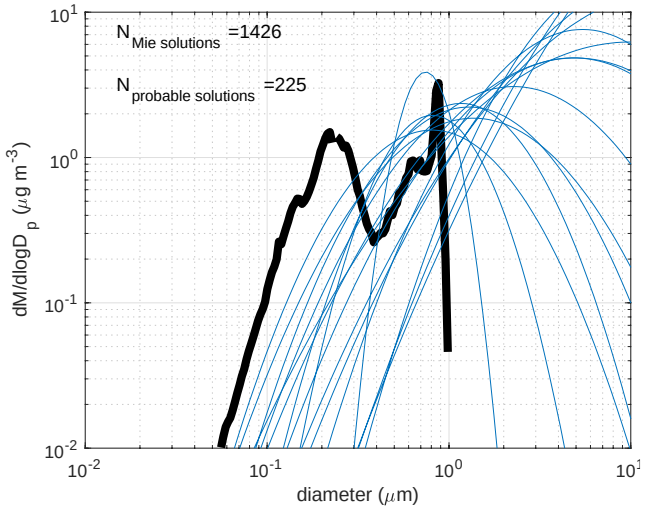

Figure S4. Sea spray mode Mie solutions that fall below the retrieval-specific scattering error threshold ($\Delta\sigma_{sca,RGB}$; $N_{Mie\ solutions}$). The retrieval presented is for the 2-h average beginning 3 December 2016 22:00 UTC. 1 in every 30 low error Mie solutions are shown to reduce clutter. The size of the reduced solution space for the most probable Mie solutions (Section 3.2) is identified as $N_{probable\ solutions}$.

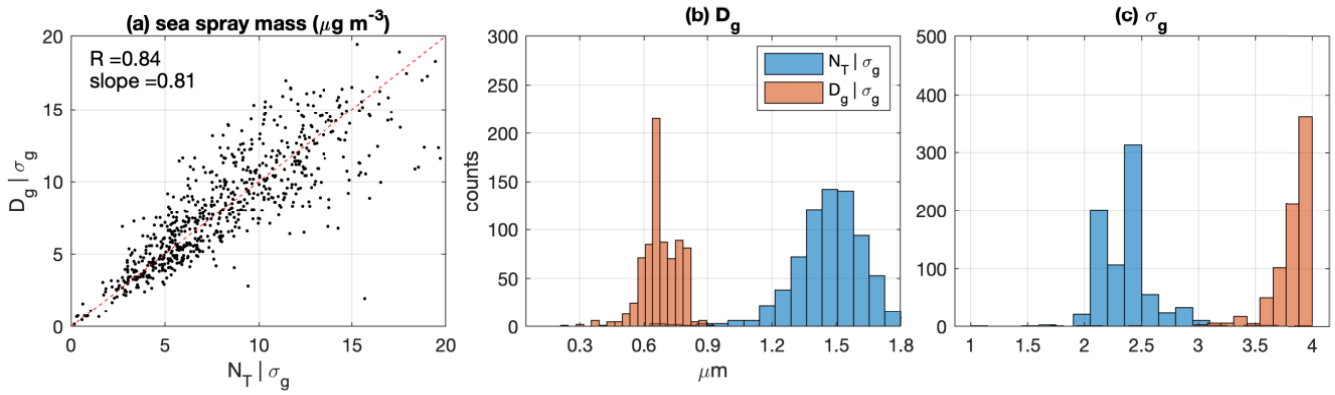

115

Figure S5. Comparisons of retrieved (a) sea spray mass, (b) sea spray mode mass mean diameter (μm), and (c) sea spray mode width for joint probability combinations of $N_T \mid \sigma_g$ and $D_g \mid \sigma_g$ applied to low error Mie solutions. In panel (a), the dashed red line symbolizes a 1:1 line.

Table S1. Refractive index (*m*) values of sea salt under various relative humidity conditions.

Refractive Index (*m*)	**Relative Humidity (RH)**	**Reference**	**remark**
1.5 + 0i	"dry"	Bi et al. (2018)	
1.45 + 10^{-8}i	66%		
1.42 + 10^{-7}i	71%		
1.39 + 10^{-9}i	76%		
1.56 + 0i	<40%	Saliba et al. (2019)	Assumed NaCl
1.51 + 10^{-7}i	"dry"	Randles et al. (2004)	Organic – inorganic mixture
1.54 + 0i	"dry"	Wang and Rood (2008)	NaCl

120

Table S2. Effects of refractive index changes on sea spray size distribution fit parameters and tracer correlations.

m	sea spray mass (µg m^{-3})	$D_{g,mass}$ (µm)	σ_g	< 1 µm sea spray mass correlation (R) with < 1 µm Cl	< 10 µm sea spray mass correlation (R) with <10 µm scattering	< 10 µm sea spray mass correlation (R) with wind speed	Average fit residual to UHSAS
1.4+0i	8.03 ± 3.65	1.42 ± 0.16	2.3 ± 0.2	0.30	0.82	0.16	1.25 ± 0.83
1.45+0i	8.37 ± 4.07	1.47 ± 0.17	2.4 ± 0.3	0.35	0.84	0.20	1.26 ± 0.89
1.5+0i	8.89 ± 3.85	1.47 ± 0.16	2.4 ± 0.2	0.34	0.85	0.20	1.26 ± 0.90
1.55+0i	8.92 ± 3.30	1.5 ± 0.15	2.4 ± 0.2	0.31	0.84	0.20	1.26 ± 0.85
1.6+0i	9.26 ± 4.19	1.52 ± 0.17	2.46 ± 0.3	0.31	0.83	0.17	1.26 ± 0.83

Table S3. Dry sea spray and water densities.

ρ	g cm^{-3}	reference	remark
(dry) sea spray ($\rho_{sea\ spray}$)	2.17	Carper (1999)	NaCl particle density.
	2.025	Saliba et al. (2019)	Average observationally-constrained estimate of sea spray particle density from merger of marine size distributions and evaluation with salt mass. Value consistent with ~20% NaCl and lower density materials (organics, other marine salts).
	2.017	Zieger et al. (2017)	Measured dry density of inorganic sea salt.
	2.2	Chin et al. (2002) Varlas et al.(2021)	Used for GOCART model simulation and optical property validation of sea salt aerosol.
water (ρ_{water})	1	Carper (1999)	

Table S4. Reported efflorescence "branch" hygroscopicity solute mass fractions at relative humidity (RH) within the range of nephelometer average and uncertainty (55 ± 10%).

solute mass fraction (ε_m)			reference
ε_m	RH	solute	
0.28	65%	NaCl	Tang et al. (1997)
0.33	55%		
0.4	45%		
0.31	65%	$NaCl – Na_2SO_4 – NaNO_3$	Tang and Munkelwitz (1994)
0.35	55%		
0.5	45%		
0.4	65%	64% wt NaCl, 34% wt KCl	Ansari and Pandis (1999)
0.45	65%	Na_2SO_4-NaCl	
0.55	55%		
0.4	65%[a]	NaCl + glycerol	Choi and Chan (2002)
0.5	55% [a]		
0.6	45% [a]		
0.55	65% [a]	NaCl + succinic acid	
0.6	55% [a]		
>0.7	45% [a]		

[a]water activity ≅ RH.

Table S5. Mass fractions of sea spray ($\varepsilon_{m,sea\ spray}$) and water ($\varepsilon_{m,water}$) and the estimated solution density (ρ) using the mass-based mixing rule Eq. (S2).

assumed RH [a]	45%	55%	65%
$\varepsilon_{m,sea\ spray}$	0.5	0.4	0.3
$\varepsilon_{m,water}$ [b]	0.5	0.6	0.7
ρ (g cm^{-3})[c]	1.4	1.3	1.2

[a]based on reported values in Table S4.

[b]Two component mixture, i.e. $\varepsilon_{m,water} = 1 - \varepsilon_{m,sea\ spray}$.

[c]assumes homogenous sea spray particles with density equal to the average of reported values (2.103 g cm^{-3}; Table S3) and water density of 1.0 g cm^{-3}.

Table S6. Sea spray size distribution modal parameters.

ρ ($g\ cm^{-3}$)	sea spray mass ($\mu g\ m^{-3}$)	D_g (μm)	σ_g
1.2	7.93 ± 3.5	1.42 ± 0.15	2.3 ± 0.2
1.3	8.37 ± 4.1	1.47 ± 0.17	2.4 ± 0.3
1.4	8.98 ± 3.8	1.5 ± 0.15	2.4 ± 0.3

140

Table S7. Sea spray tracer correlations for different fit RSS thresholds.

Fit RSS threshold	$N_{samples}$	< 1 µm sea spray mass correlation (R) with < 1 µm Cl	< 10 µm sea spray mass correlation (R) with wind speed
1	375	0.27	0.17
2	639	0.31	0.17
3	740	0.31	0.19
4	775	0.32	0.20
5	794	0.33	0.20
6	800	0.33	0.19
7	808	0.32	0.19
8	811	0.31	0.18
9	817	0.31	0.17
10	825	0.31	0.18

References

Ansari, A. and Pandis, S.: Prediction of multicomponent inorganic atmospheric aerosol behavior, Atmospheric Environment, 33, 745-757, 10.1016/S1352-2310(98)00221-0, 1999.

Bi, L., Lin, W., Wang, Z., Tang, X., Zhang, X., and Yi, B.: Optical Modeling of Sea Salt Aerosols: The Effects of Nonsphericity and Inhomogeneity, Journal of Geophysical Research-Atmospheres, 123, 543-558, 10.1002/2017JD027869, 2018.

Carper, J.: The CRC Handbook of Chemistry and Physics, Library Journal, 124, 192-+, 1999.

Chin, M., Ginoux, P., Kinne, S., Torres, O., Holben, B., Duncan, B., Martin, R., Logan, J., Higurashi, A., and Nakajima, T.: Tropospheric aerosol optical thickness from the GOCART model and comparisons with satellite and Sun photometer measurements, Journal of the Atmospheric Sciences, 59, 461-483, 10.1175/1520-0469(2002)059<0461:TAOTFT>2.0.CO;2, 2002.

Choi, M. and Chan, C.: The effects of organic species on the hygroscopic behaviors of inorganic aerosols, Environmental Science & Technology, 36, 2422-2428, 10.1021/es0113293, 2002.

de Faria, J., Bundke, U., Freedman, A., Onasch, T., and Petzold, A.: Laboratory validation of a compact single-scattering albedo (SSA) monitor, Atmospheric Measurement Techniques, 14, 1635-1653, 10.5194/amt-14-1635-2021, 2021.

Delene, D. and Ogren, J.: Variability of aerosol optical properties at four North American surface monitoring sites, Journal of the Atmospheric Sciences, 59, 1135-1150, 10.1175/1520-0469(2002)059<1135:VOAOPA>2.0.CO;2, 2002.

Di Biagio, C., Formenti, P., Balkanski, Y., Caponi, L., Cazaunau, M., Pangui, E., Journet, E., Nowak, S., Andreae, M., Kandler, K., Saeed, T., Piketh, S., Seibert, D., Williams, E., and Doussin, J.: Complex refractive indices and single-scattering albedo of global dust aerosols in the shortwave spectrum and relationship to size and iron content, Atmospheric Chemistry and Physics, 19, 15503-15531, 10.5194/acp-19-15503-2019, 2019.

Haywood, J., Francis, P., Osborne, S., Glew, M., Loeb, N., Highwood, E., Tanre, D., Myhre, G., Formenti, P., and Hirst, E.: Radiative properties and direct radiative effect of Saharan dust measured by the C-130 aircraft during SHADE: 1. Solar spectrum, Journal of Geophysical Research-Atmospheres, 108, 10.1029/2002JD002687, 2003.

Muller, T., Schladitz, A., Kandler, K., and Wiedensohler, A.: Spectral particle absorption coefficients, single scattering albedos and imaginary parts of refractive indices from ground based in situ measurements at Cape Verde Island during SAMUM-2, Tellus Series B-Chemical and Physical Meteorology, 63, 573-588, 10.1111/j.1600-0889.2011.00572.x, 2011.

Randles, C., Russell, L., and Ramaswamy, V.: Hygroscopic and optical properties of organic sea salt aerosol and consequences for climate forcing, Geophysical Research Letters, 31, 10.1029/2004GL020628, 2004.

Saliba, G., Chen, C., Lewis, S., Russell, L., Rivellini, L., Lee, A., Quinn, P., Bates, T., Haentjens, N., Boss, E., Karp-Boss, L., Baetge, N., Carlson, C., and Behrenfeld, M.: Factors driving the seasonal and hourly variability of sea-spray aerosol number in the North Atlantic, Proceedings of the National Academy of Sciences of the United States of America, 116, 20309-20314, 10.1073/pnas.1907574116, 2019.

TANG, I. and MUNKELWITZ, H.: AEROSOL PHASE-TRANSFORMATION AND GROWTH IN THE ATMOSPHERE, Journal of Applied Meteorology, 33, 791-796, 10.1175/1520-0450(1994)033<0791:APTAGI>2.0.CO;2, 1994.

Tang, I., Tridico, A., and Fung, K.: Thermodynamic and optical properties of sea salt aerosols, Journal of Geophysical Research-Atmospheres, 102, 23269-23275, 10.1029/97JD01806, 1997.

Varlas, G., Marinou, E., Gialitaki, A., Siomos, N., Tsarpalis, K., Kalivitis, N., Solomos, S., Tsekeri, A., Spyrou, C., Tsichla, M., Kampouri, A., Vervatis, V., Giannakaki, E., Amiridis, V., Mihalopoulos, N., Papadopoulos, A., and Katsafados, P.: Assessing Sea-State Effects on Sea-Salt Aerosol Modeling in the Lower Atmosphere Using Lidar and In-Situ Measurements, Remote Sensing, 13, 10.3390/rs13040614, 2021.

Von Hoyningen-Huene, W., Dinter, T., Kokhanovsky, A., Burrows, J., Wendisch, M., Bierwirth, E., Muller, D., and Diouri, M.: Measurements of desert dust optical characteristics at Porte au Sahara during SAMUM, Tellus Series B-Chemical and Physical Meteorology, 61, 206-215, 10.1111/j.1600-0889.2008.00405.x, 2009.

Wang, W. and Rood, M.: Real refractive index: Dependence on relative humidity and solute composition with relevancy to atmospheric aerosol particles, Journal of Geophysical Research-Atmospheres, 113, 10.1029/2008JD010165, 2008.

Wu, H., Taylor, J., Szpek, K., Langridge, J., Williams, P., Flynn, M., Allan, J., Abel, S., Pitt, J., Cotterell, M., Fox, C., Davies, N., Haywood, J., and Coe, H.: Vertical variability of the properties of highly aged biomass burning aerosol transported over the southeast Atlantic during CLARIFY-2017, Atmospheric Chemistry and Physics, 20, 12697-12719, 10.5194/acp-20-12697-2020, 2020.

Zieger, P., Vaisanen, O., Corbin, J., Partridge, D., Bastelberger, S., Mousavi-Fard, M., Rosati, B., Gysel, M., Krieger, U., Leck, C., Nenes, A., Riipinen, I., Virtanen, A., and Salter, M.: Revising the hygroscopicity of inorganic sea salt particles, Nature Communications, 8, 10.1038/ncomms15883, 2017.

Zuidema, P., Sedlacek, A., Flynn, C., Springston, S., Delgadillo, R., Zhang, J., Aiken, A., Koontz, A., and Muradyan, P.: The Ascension Island Boundary Layer in the Remote Southeast Atlantic is Often Smoky, Geophysical Research Letters, 45, 4456-4465, 10.1002/2017GL076926, 2018.